

RSC Advances



This is an *Accepted Manuscript*, which has been through the Royal Society of Chemistry peer review process and has been accepted for publication.

Accepted Manuscripts are published online shortly after acceptance, before technical editing, formatting and proof reading. Using this free service, authors can make their results available to the community, in citable form, before we publish the edited article. This *Accepted Manuscript* will be replaced by the edited, formatted and paginated article as soon as this is available.

You can find more information about *Accepted Manuscripts* in the [Information for Authors](#).

Please note that technical editing may introduce minor changes to the text and/or graphics, which may alter content. The journal's standard [Terms & Conditions](#) and the [Ethical guidelines](#) still apply. In no event shall the Royal Society of Chemistry be held responsible for any errors or omissions in this *Accepted Manuscript* or any consequences arising from the use of any information it contains.

Influence of Thermal and Solvent Annealing on the Morphology and Photovoltaic Performance of the Solution Processed, D-A-D type Small Molecules-Based Bulk Heterojunction Solar Cells

CH. Pavan Kumar,^{a,b} K. Ganesh,^{a,b} T. Suresh,^a Abhishek Sharma,^c K. Bhanuprakash^{a,b}, G. D. Sharma,^{*,d} Malapaka Chandrasekharam,^{*,a,b}

^aNetwork of Institutes for Solar Energy, CSIR- Indian Institute of Chemical Technology, I&PC Division, Uppal Road, Tarnaka, Hyderabad - 500 007, India.

^bAcademy of Scientific and Innovative Research, CSIR-IICT.

^cDepartment of Electronics and communication Engineering, LNMIIT, Jamdoli, Jaipur 302031.

^dR & D center for Engineering and Science, JEC group of colleges, Jaipur Engineering College campus, Jaipur, 303101, India.

E-mail: chandra@iict.res.in, gdsharma273@gmail.com

ABSTRACT:

Four new solution-processable donor-acceptor-donor (D-A-D) structured organic small molecules (**CSDPP9**, **CSDPP10**, **CSDPP11** and **CSDPP12**) with diketopyrrolopyrrole (DPP) as central core unit and different electron donating groups as the terminal units, were designed and synthesized. These molecules employed as donors along with PC₇₁BM as electron acceptor in solution processed bulk heterojunction (BHJ) solar cells, exhibited strong visible (450-650 nm) absorption band with suitable molecular orbital energy levels. OSCs based on these small molecules achieved moderate power conversion efficiency (PCE) in the range of 2.86-3.55 % along with high open circuit voltage (V_{oc}) and the difference is correlated with the different electron donating unit used in the DPP. The observed high open circuit voltage (V_{oc}) of the device is directly related with the HOMO energy level of the DPP. The BHJ devices, based on **CSDPP11**:PC₇₁BM and **CSDPP12**:PC₇₁BM subjected to solvent and thermal annealing showed improved PCE of 5.47 % and 4.88 % respectively. The enhancement in the PCE has been attributed to the improved charge carrier mobility, crystallinity and light harvesting ability of active layer.

KEY WORDS: solution processed small molecules, diketopyrrolopyrrole (DPP), organic solar cells, thermal annealing, solvent annealing, B3LYP/6-311 G(d,p) level theory.

INTRODUCTION

Organic solar cells (OSCs) have been evolving into promising alternative to conventional silicon based solar cells owing to their advantages such as easy processing, light-weight, low cost and flexibility.¹⁻⁴ Significant recent advancements in the power conversion efficiency (PCE) of OSCs have been reported and a PCE of over 10% have been achieved through careful material design and device optimization.⁵⁻¹¹ The PCEs of OSCs got a major boost with the introduction of bulk heterojunction (BHJ) concept, consisting of an interpenetrating network, where exciton dissociation takes place at the interface of donor and acceptor materials and is driven by the energy level gaps of the molecular orbitals (i.e. HOMO of donor and LUMO of acceptor).^{12,13} Further the free charge carriers, move towards the respective electrodes to generate photocurrent. Solution-processable narrow-bandgap small molecules have gained increasing attention because of their advantages, such as defined molecular structure, intrinsic monodispersity, high purity, negligible batch-to-batch variations, and reproducible performance, compared to conventional polymer counterparts.¹⁴⁻¹⁷ Small molecules OSCs (SMOSCs) have also achieved a high PCE of ~9-10 %¹⁸⁻²⁰, which is almost equal to that for polymer solar cells, indicating the their potential. To date an impressive PCE of 12 % has been achieved for a vacuum processed triple junction tandem solar cell based on small molecules.²¹

It is well known that the molecular configuration of the donor material play an important role in the photovoltaic properties of SMOSC devices because the donor backbone controls the bandgap, energy levels and light harvesting ability of the materials employed.²² The current research in search of new small molecules systems resulted in the development of a large variety of promising organic materials with different donor (D)-acceptor (A) subunit combinations. In such D-A structured organic semiconductors, the intramolecular charge transfer transitions can effectively reduce the bandgap. For example, symmetrical acceptor – donor – acceptor (A-D-A)²³⁻²⁵ and donor-acceptor-donor (D-A-D)²⁶⁻³¹ based small molecules have been developed with PCE approaching those of the polymeric counterpart. The backbone engineering, the alkyl chain engineering can greatly manipulate the solubility, crystallization, intra- and intermolecular forces, and the film morphology of the blend films, which can effectively improve the photovoltaic efficiency. Recent reports have shown that the device performance depends upon the alkyl chain length, position, branching point, symmetry, chirality and density.³²⁻³⁴

In addition to the backbone and alkyl-chain design, modulation of the molecular backbone by end-capping with electron donating or withdrawing aromatic groups is important not only for improving the molecular optoelectronic properties but also to control aggregation of the materials.^{22,33-40} Among the vast variety of the electron withdrawing units developed, the diketopyrrolopyrrole (DPP) unit is promising for the design of D-A materials due to their advantages such as strong light absorption, photostability, and the convenience of large scale synthesis.^{41,42} The planar skeleton of DPP and its ability to readily form hydrogen bonds facilitate π - π stacking, which is beneficial to obtain high mobility.⁴³⁻⁴⁵ As a strong electron withdrawing moiety, DPP has been coupled with a variety of electron donating groups to provide low bandgap conjugated polymers and small molecules for BHJ OSCs.^{46,47} BHJ OSCs exhibited PCEs as high as in the range of 6.5% - 8.8% for DPP based polymers⁴⁸⁻⁵⁰ and 5.8 % for small molecules.^{51,52} Thus DPP materials functionalized with a D-A-D structure have potential application for SMOSCs.

Owing to our continued interest in the synthesis of new small molecules as donors for BHJ solar cells, we recently reported two simple D-A-D structured DPP molecules (CSDPP1 and CSDPP3) with indole and 2,4,6-triisopropylphenyl as terminal donors and the test cells based on CSDPP1:PC70BM blend achieved a PCE of 4.91%.²⁸ To examine the effect of novel aromatic donor units on the properties of DPP based molecules, we successfully synthesized a series of D-A-D structured small molecular donors, all of which contain thiophene ended DPP as central core and different donors i.e. mesitylene (**CSDPP9**), 1-isopropoxy-2-methylbenzene (**CSDPP10**), 1,2,3-trimethoxy-5-methylbenzene (**CSDPP11**) and 1,3-di-*tert*-butylbenzene (**CSDPP12**) as arms shown in Figure 1. Their photophysical and electrochemical properties show that they harvest sunlight across the entire visible spectrum range and have appropriate energy levels for efficient exciton dissociation in solution processed OSCs. Therefore we explored the photovoltaic properties of the new DPP based small molecules as donor along with the PC₇₁BM as acceptor for BHJ solar cells with the device structure ITO/PEDOT:PSS/donors:PC₇₁BM/Au. The PCE for the devices **CSDPP9**, **CSDPP10**, **CSDPP11** and **CSDPP12** as donor was about 2.86 %, 2.89 %, 3.55 % and 3.05 %, respectively. To further improve the PCE of the devices, we have used a two step treatment i.e. thermal annealing (TA) and subsequent solvent annealing (SATA) treatment to optimize the morphology and achieved PCE of 5.47 % and 4.88 % for **CSDPP11**:PC₇₁BM and **CSDPP12**:PC₇₁BM active layers, respectively.

RESULTS AND DISCUSSION

Synthesis of CSDPP 9-CSDPP12.

The synthetic route to **CSDPP9-CSDPP12** sensitizers were depicted in scheme 1 (Supporting Information). The core DPP (**1**) was synthesized according to the literature procedure⁵³ followed by N-alkylation with 2-ethylhexylbromide to afford pure compound **2**. Compound **2** was subjected to bromination with NBS to afford compound **3**. The target sensitizers **CSDPP9-CSDPP12** were prepared employing the Pd(PPh₃)₄ assisted Suzuki coupling reaction of compound **3** in 48-58% yields respectively.

Optical and Electrochemical properties.

The optical properties of **CSDPP9-CSDPP12** were first investigated in dilute DCM solution. The UV-visible absorption spectra of these DPPs in solution are shown in Figure 2(a). All four **CSDPPs** showed different absorption peaks indicating that the end capped group exerts influence on the intrinsic electronic properties of chromophore or their solution phase conformations. Three maxima are observed in the UV-visible region. The high energy absorption band (λ_{max}) around 384 nm corresponds to a π - π^* transition for both thiophene and central DPP units,^{54,55} while the absorption band in low energy region ($\lambda_{\text{max}} = 561 \text{ nm}, 579 \text{ nm}, 609 \text{ nm}$ and 597 nm for **CSDPP9**, **CSDPP10**, **CSDPP11** and **CSDPP12**) is assigned to the intramolecular charge transfer (ICT) between the end capped donor and central DPP units. The different ICT absorption peak may be attributed to the different electron donating ability of end capped donor moieties. The extinction coefficient for these DPPs also varies, indicating the end capped unit also influences the light harvesting property. All these DPP molecules exhibit impressive light harvesting ability in solution with maximum molar extinction coefficient ($\epsilon_{\text{max}} = 5.7 - 8.4 \times 10^4 \text{ M}^{-1} \text{ cm}^{-1}$).

The absorption spectra of **CSDPPs** thin film spin cast from DCM solution on glass substrate are shown in Figure 2(b). All the films show a peak around 415 nm that has been attributed to a π - π^* transition for both thiophene and central DPP units.⁵² In addition, intense absorptions are found in the wavelength region 500 - 700 nm. Relative to absorptions in solution, thin films of all **CSDPPs** are remarkably red shifted and broadened, which is caused by intermolecular π - π stacking. The relative intensities and positions of the absorption peaks are related to crystal packing, as peaks arise from both intra-and intermolecular charge transfer. Compared to the corresponding solution spectrum, the absorption edge extends to 660 nm, 682 nm, 712 nm, 698 nm respectively in solid state film. The absorption ranges of **CSDPP11** and **CSDPP12** are broader than that of **CSDPP9** and **CSDPP10**, which indicates that the size of

end groups have a significant influence on the molecular ordering and π - π stacking in thin film. The optical bandgap calculated from the film absorption edge is 1.88 eV, 1.82 eV, 1.74 eV and 1.78 eV for **CSDPP9**, **CSDPP10**, **CSDPP11** and **CSDPP12**, respectively.

To gain a better understanding of the structure–property relationships, we have carried out TDDFT studies of these molecules in the solvent DCM using B3LYP level of theory. The TDDFT results with B3LYP are in nearly good agreement with experimental UV-Vis spectra. The spectra have been produced by convoluting Gaussian functions with FWHM = 0.35 eV centered at the excitation wave numbers. The normalized plots of simulated and experimental UV-Vis spectra of **CSDPPs** are depicted in Figure S2. The wavelengths of the excitations with the largest oscillator strengths (f) within these bands are given in Table 4. The intense singlet transition is a HOMO to LUMO transition at 534 nm ($f=0.7576$) for **CSDPP9**, 577 nm ($f=1.0716$) for **CSDPP10**, 598 nm ($f=1.1644$) for **CSDPP11** and 585 nm ($f=1.0614$) for, **CSDPP12**. The optimized geometry parameters, at the B3LYP/6-311 G(d,p) level of theory are shown in supporting information.

The energy levels i.e. HOMO and LUMO of the organic semiconducting material are crucial for governing the overall performance of OSCs.⁵⁶ The HOMO energy level was calculated from the onset oxidation potential observed in cyclic voltammogram, assuming that energy level of ferrocene/ferrocenium (Fc/Fc⁺) to be -4.80 eV below the vacuum level (Figure 3 (a)). The formal potential of Fc/Fc⁺ was measured as 0.1 V vs Ag/AgCl which has an absolute energy level of -4.70 eV relative to the vacuum level for calibration. The LUMO energy level of the **CSDPPs** was estimated from LUMO= HOMO- E_{0-0} , where E_{0-0} estimated from the intersection of absorption and emission spectrum in solution. The values of HOMO and LUMO energy levels are summarized in Table 1. It can be seen from the Table 1 that the LUMO energy level of all **CSDPPs** are almost same, whereas the differences in HOMO energy levels are attributed to the different end capping units of same DPP core acceptor. Moreover, the trend in the variation of HOMO energy levels is consistent with the trends in the electron donating ability of the donor units. For effective charge separation and transfer from D to A, the LUMO level of donor needs to be 0.3-0.5 eV higher than the LUMO level of acceptor.^{57,58} In line with this, the higher LUMO level of **CSDPPs** (~-3.5 eV) than that of PC₇₁BM (-4.1 eV) indicates that all these small molecules are suitable candidates (Figure 3 (b)) as donor materials in OSCs when blended with PC₇₁BM acceptor facilitating photoinduced charge separation possible at D/A interface. The deeper HOMO level of these new compounds is

beneficial to higher V_{oc} of OSCs, since V_{oc} is generally proportional to the difference between the LUMO energy level of the acceptor and the HOMO energy level of donor.^{15,59}

We have plotted the isosurfaces (isovalue=0.02) of the HOMO and LUMO (Figure S3), as well as the nearest frontier orbitals of **CSDPPs** which are involved in transitions with strong contributions to the first excitation as well as to next two excitations with strong oscillator strength. To gain further insight into the electron density distribution in each molecule, partial electron density contribution and terminal moieties in each molecule from the respective frontier orbitals have been generated and depicted in Figure S4. For all of the **CSDPPs** the HOMO and LUMO extend at least over all of their main inner body up to thiophene moieties. The HOMO-2 is localized at various degrees over the whole of the structure while LUMO+2 majorly localized over the terminating groups. We partition the structures into the diketopyrrolopyrrole (**DKPP**), alkyl moieties, the thiophene moieties (**Th**), and the benzene-derived terminating groups which are trimethylbenzene (**TMB**), methylisopropoxybenzene (**MIPOB**), trimethoxybenzene (**TMOB**), and the *ditert*-butylbenzene (**DTBB**) for **CSDPP9**, **CSDPP10**, **CSDPP11** and **CSDPP12** respectively. The HOMO of **CSDPPs** is dominated by contributions from the **DKPP** and **Th** groups by 68%, 56%, 54%, 59% and 29%, 30%, 31%, 31% respectively, with only minor contribution 2%, 13%, 15%, and 10% from the **TMB**, **MIPOB**, **TMOB** and **DTBB** moieties. The LUMO of **CSDPPs** have very similar contributions to the HOMO from the **DKPP** (60%, 56%, 53% and 54%), **Th** (38%, 37%, 36% and 37%) and terminal groups by (2%, 7%, 10% and 10%) respectively.

The calculated HOMO, LUMO energies and the HOMO-LUMO gap (HLG) at a B3LYP/6-311g(d,p) level in DCM solvent is given in Figure 4. The computationally and experimentally determined HOMO, LUMO energies are in good agreement. The HOMO-LUMO gaps are shown in Table 2.

Photovoltaic properties.

In BHJ OSCs, the relative amounts of the donor and acceptor materials used in the BHJ active layer is of great importance for the observed photovoltaic performance, since there should be a balance between absorbance and charge transport network of active layer. When acceptor content is too high, the absorbance and hole transport ability in the active layer will be decreased, while when the acceptor content is too low, the electron transporting ability will be limited. To evaluate the photovoltaic performance of DPP small molecules, OSC are fabricated with a different donor to acceptor ratio, using the conventional device architecture ITO/PEDOT:PSS/blends/Au. The blends were prepared using DCM solution with a total concentration of 20 mg/mL. After optimizing the ratio of donor to acceptor, the best results

were found for the ratio of 1:1 w/w for all DPPs. The current –voltage characteristics of the devices, under illumination, for optimized blend ratio are shown in Figure 5a and corresponding photovoltaic parameters are summarized in Table 3. **CSDPP9** based device showed photovoltaic performance with a V_{oc} of 1.02 V, a J_{sc} of 7.38 mA/cm², FF of 0.38 and a PCE of 2.86 %. The device based on **CSDPP10** showed PCE of 2.88 % with J_{sc} of 7.68 mA/cm², V_{oc} of 0.94 V and FF of 0.40. The devices of **CSDPP11** and **CSDPP12** showed PCE of 3.55 % (J_{sc} = 9.18 mA/cm², V_{oc} = 0.88 V and FF = 0.44) and 3.05 % (J_{sc} = 8.12 mA/cm², V_{oc} = 0.94 V and FF = 0.40). The V_{oc} of the devices are consistent with the respective values of HOMO levels of DPPs, since the V_{oc} of BHJ OSCs is directly proportional to the difference in the HOMO energy level of donor and LUMO energy level of the acceptor used in the BHJ active layer. The deepest HOMO energy level of the **CSDPP9** is attributed to the highest V_{oc} of 1.02 V for the device with **CSDPP9**:PC₇₁BM blend. The highest value of J_{sc} for the device with **CSDPP11**:PC₇₁BM blend may be attributed to the low band gap of **CSDPP11** and broader absorption profile.

The external quantum efficiency (EQE) of the BHJ OSCs based on **CSDPP9-CSDPP12** and PC₇₁BM were also measured under monochromatic light and the results are shown in Figure 5b. All the curves exhibit a broad response in the wavelength region 350-700 nm and closely resemble with the absorption spectra of the respective blends. The J_{sc} values estimated from the integration of EQE spectrum of the corresponding devices are in close agreement with values obtained from the corresponding J-V characteristics under illumination.

To get information about the different values of J_{sc} for devices based on these DPPs as donor, we have measured the hole mobilities of the devices by fabricating the hole only devices i.e., ITO/PEDOT:PSS/ active layer/Au and then measured their J-V characteristics in dark (Figure 6). Using the space charge limited current model (SCLC), the estimated values of hole mobility for **CSDPP9**, **CSDPP10**, **CSDPP11** and **CSDPP12** are 2.34×10^{-6} , 2.56×10^{-6} , 6.78×10^{-6} and 4.67×10^{-6} cm²/Vs, respectively. The trends of the hole mobility is consistent with the observed values of J_{sc} and FF.

The V_{oc} of these devices is quite high but the values of J_{sc} and FF are rather low, may be arising from poor and unoptimized morphology of the DPP:PC₇₁BM blend film. To further improve their photovoltaic properties, we have used a simple two step annealing (TSA) approach involving thermal and solvent vapor annealing to optimize the morphology of the blend thin film as reported in literature.^{60,61} We have used only **CSDPP11** and **CSDPP12** for this investigation, since they have higher PCE than the other two. First, the blended thin film as cast from DCM solution on PEDOT:PSS was heated on a hot plate at 80 °C for 10 minutes, i. e.,

thermal annealing (TA). After cooling to room temperature, the film was placed in a glass petri dish containing 200 μL THF for 2 minutes for solvent annealing (SATA). The J-V characteristics of the device are shown in Figure 6 and 7 for **CSDDP11:PC₇₁BM** and **CSDPP12:PC₇₁BM** blends, respectively and the corresponding photovoltaic parameters are compiled in Table 4. The device based on TA showed PCE of 4.63 % ($J_{\text{sc}} = 9.98 \text{ mA/cm}^2$, $V_{\text{oc}} = 0.86 \text{ V}$ FF = 0.54) and 4.15 % ($J_{\text{sc}} = 8.88 \text{ mA/cm}^2$, $V_{\text{oc}} = 0.90 \text{ V}$ FF = 0.52) for **CSDPP11:PC₇₁BM** and **CSDPP12:PC₇₁BM** active layers, respectively. After the SATA treatment, the performance was further improved to PCE of 5.47 % ($J_{\text{sc}} = 10.86 \text{ mA/cm}^2$, $V_{\text{oc}} = 0.84 \text{ V}$, FF = 0.60) and 4.88 % ($J_{\text{sc}} = 9.92 \text{ mA/cm}^2$, $V_{\text{oc}} = 0.88 \text{ V}$, FF = 0.56) for **CSDPP11:PC₇₁BM** and **CSDPP12:PC₇₁BM** active layers, respectively. The improvement in the PCE has been mainly resulting from the significant enhancement in both J_{sc} and FF, may be originated from the enhanced absorption, better active layer morphology and higher and more balanced charge carrier mobilities.

To get more insight information about the improved photovoltaic performance of the devices, with TA and SATA treatment of active layers, we have investigated the UV-Visible absorption spectra of active layers (Figure 9) and EQE spectra (Figure 7 and 8) of corresponding devices. As shown in Figure 9, the absorption spectrum of TA treated blend film showed a redshift and a shoulder peak at 657 nm, as compared to the absorption spectrum of as cast film, which is related to the enhanced π - π stacking between the molecule backbones.^{62,63} For the films with further solvent annealing SATA treatment, the absorption intensity further improved. The EQE spectra of the devices are shown in Figure 7 and 8. It can be seen that there is a uniform increase in the EQE values across the whole wavelength range for the devices with TA treatment and further improved with SATA treatment. These results are consistent with the trends of UV-visible absorption spectra of the blends. The calculated J_{sc} values from the integration of the EQE spectra of the devices are 9.83 mA/cm^2 , 8.76 mA/cm^2 , 10.75 mA/cm^2 and 8.81 mA/cm^2 for **CSDPP11:PC₇₁BM** (TA), **CSDPP12:PC₇₁BM** (TA), **CSDPP11:PC₇₁BM** (SATA) and **CSDPP12:PC₇₁BM** (SATA) based blends, respectively.

The series resistance (R_s) and shunt resistance (R_{sh}) of the devices estimated from the slope of J-V characteristics of devices, under illumination at V_{oc} and J_{sc} , respectively are compiled in the table 3 and 4. The small R_s for TA or SATA treated cells indicate a slower charge recombination and small dark current. Hence the small R_s suggest that either TA or SATA treatment allows effective suppression of recombination in the device and lower the charge transport resistance. On the other hand, the larger value of R_{sh} for the devices based on

TA or SATA treated active layers indicates that the reverse saturation current (J_0) is smaller, resulting in higher FF. As can be seen from table 3 and 4, the V_{oc} slightly decreases with either TA or SATA treatment. The intermolecular interaction (or electronic coupling) between the donor and acceptor materials used in blended active layer has a significant influence on the J_{sc} and V_{oc} .^{64,65} The decreased V_{oc} of the devices based on TA and SATA treated blend films could be due to the increased intermolecular interaction between the donor and acceptor.

The charge transport within the active layer plays an important role for the photocurrent generation in the devices. The hole mobilities of the thin films have been measured by SCLC method (Figure 10a and 10b) from the J-V characteristics and are compiled in the table 3. The hole mobilities of the blended active films with TA and SATA treatments are increased significantly as compared to those untreated. The increase in hole mobilities of blended thin film with TA and SATA treatments may be due to the better packing of **CSDPP11** in the films as observed in the XRD data.

In order to get information on the influence of these treatments on packing and crystallinity of active layers, we have used x-ray diffraction (XRD) analysis. As shown in Figure 11, the as cast **CSDPP11**:PC₇₁BM blend film shows a weak diffraction peak (100) at $2\theta = 6.04^\circ$. In the TA treated blend film, the intensity of this peak significantly increased and further increased with SATA treatment. These results indicate that TA treatment of blend layer leads to the better organized assembly and crystallinity of **CSDPP11** donor phase^{66,67} which would benefit the charge transport.⁶⁸ Similar influence of TA and SATA has been observed for **CSDPP12**:PC₇₁BM blend.

The TEM images also show the differences between the morphology of the **CSDPP11**:PC₇₁BM blend with and without TA and SATA treatments (Figure 12). A similar TEM image has been observed for **CSDPP12**:PC₇₁BM blend films. As shown in Figure 12 the untreated blend film, shows poor interpenetrating networks with low domain sizes between the donor and acceptor phases. After the TA treatment, the interpenetrating network improves and further improves with SATA treatment with width of 20-25 nm, which is comparable to exciton diffusion length.^{69,70} The better morphology and optimized interpenetrating networks of blend active layer films with TA and SATA treatment leads to increased donor-acceptor interfacial area and hole mobility, which may increase the exciton dissociation and charge transport efficiency and reduces the charge carrier recombination, thus higher J_{sc} and FF.^{63,71}

CONCLUSIONS

Four DPP derivatives with same DPP acceptor core and different donor end capping units were synthesized. The solution processed BHJ solar cells based on these small molecules as donors along with PC₇₁BM as electron acceptor showed moderate PCE in the range of 2.86 - 3.55 %. The V_{oc} of these devices is quite high and is well consistent with their HOMO energy level. After the optimization of morphology of active layer with SATA treatment, the PCE of devices based on **CSDPP11**:PC₇₁BM and **CSDPP12**:PC₇₁BM improved up to 5.47 % and 4.88 %, respectively. The improvement is attributed to the combined effect of better morphology and crystallinity of active layer, enhanced light harvesting ability and charge carrier mobility, induced by the TA and SATA treatment of the active layer.

EXPERIMENTAL DETAILS

Device fabrication and characterization

The BHJ OSCs were fabricated using the indium tin oxide (ITO) coated glass substrate as anode, Au as cathode and a blended film of **CSDPP9** or **CSDPP10** or **CSDPP11** or **CSDPP12**:PC₇₁BM between the two electrodes as photoactive layer as follows: Firstly, ITO coated glass was precleaned, with detergent, ultrasonicated in acetone and isopropyl alcohol respectively, and subsequently dried in an oven for 12 hr. An aqueous solution of PEDOT:PSS (Heraeus, Clevious P VP, Al 4083) was spin cast on the ITO substrates obtaining a film of about 40 nm thick. The PEDOT:PSS film was then dried for 10 min at a temperature of 120 °C in ambient conditions. Then, a 20 mg/mL solution of **CSDPP9** or **CSDPP10** or **CSDPP11** or **CSDPP12**:PC₇₁BM blends in DCM solution were prepared with different weight ratio and then spun cast on the top of PEDOT:PSS layer and then dried in air. The blend was thermally annealed at 80 °C for 10 min (TA treatment). After cooling down to room temperature, the blends were treated with THF solution (solvent annealing) (SATA treatment). The thickness of the photoactive layer is about 100 ± 10 nm. Finally ~ 90 nm thick Au electrode was deposited on the top of BHJ film under reduced pressure (<10⁻⁶ Torr). All the devices were fabricated and tested in ambient atmosphere without encapsulation. The active area of the devices is about 20 mm².

The current–voltage characteristics of the devices were measured using a computer controlled Keithley 238 source meter in dark as well as under illumination intensity of 100 mW/cm². A xenon light source coupled with AM1.5 optical filter was used as light source to illuminate the surface of the devices. The external quantum efficiency (EQE) of the devices

was measured illuminating the device through the light source and monochromator and resulting current was measured using Keithley electrometer under short circuit condition.

Computational Details

All the calculations have been performed using the Gaussian 09 program package.⁷² Geometrical optimization was performed in vacuo using B3LYP^{73,74} exchange-correlation functional and a 6-311G(d, p) basis set.⁷⁵ The optimized geometries were then used to obtain frontier molecular orbitals (FMOs). To simulate the optical spectra, the lowest spin allowed singlet–singlet transitions were computed on the ground state geometry. TDDFT calculations of the lowest singlet–singlet excitations were performed in DCM solution, on the optimized geometries using the B3LYP/6-311G (d, p) level of theory. The integral equation formalism polarizable continuum model (PCM)⁷⁶ within self-consistent reaction field (SCRF) theory, has been used to describe the solvation of the molecules. The software GaussSum 2.2.5⁷⁷ was utilized to simulate the major portion of absorption spectrum and to analyze the nature of transitions. The percentage contributions of individual moieties of the dyes to the respective molecular orbitals have also been calculated.

ASSOCIATED CONTENT

*Supporting Information

Experimental details, synthetic route for **CSDPP9-CSDPP12**, ¹H and ¹³C NMR spectra, optimized geometry parameters, Comparison between experimental (black lines) and calculated (red lines) UV-Vis absorption spectra of the **CSDPP** dyes in DCM solution, structures of optimized geometries, molecular orbitals, Percentage contributions of the orbital density of the individual groups.

ACKNOWLEDGEMENTS

Ch. P.K. thanks UGC, New Delhi for a senior research fellowship. We are also thankful to Department of Physics, LNMIIT, Jaipur for providing the facilities for device fabrication and characterization. Thanks to Director, MNIT, for providing XRD and TEM facilities.

REFERENCES

- (1) P. M. Beaujuge, and J. J. M. Fréchet, *J. Am. Chem. Soc.* 2011, **133**, 20009–20029.
- (2) G. Li, R. R. Zhu, and Y. Yang, *Nat. Photonics* 2012, **6**, 153–161.
- (3) B. Walker, C. Kim, and T.-Q. Nguyen, *Chem. Mater.* 2011, **23**, 470–482.
- (4) J. Roncali, *Acc. Chem. Res.* 2009, **42**, 1719–1730.
- (5) J. E. Coughlin, Z. B. Henson, G. C. Welch, and G. C. Bazan, *Acc. Chem. Res.* 2014, **47**, 257–270.
- (6) M. A. Green, K. Emery, Y. Hishikawa, W. Warta, and E. D. Dunlop, *Prog. Photovolt: Res. Appl.* 2014, **22**, 1–9.
- (7) F. C. Krebs, N. Espinosa, M. Hösel, R. R. Søndergaard, and M. Jørgensen, *Adv. Mater.* 2014, **26**, 29–39.
- (8) C. -C. Chen, W. -H. Chang, K. Yoshimura, K. Ohya, J. You, J. Gao, Z. Hong, and Y. Yang, *Adv. Mater.* 2014, **26**, 5670–5677.
- (9) Y. Liu, J. Zhao, Z. Li, C. Mu, W. Ma, H. Hu, K. Jiang, H. Lin, H. Ade, and H. Yan *Nat. Commun.* 2014, **5**, 5293–5301.
- (10) B. Kan, M. Li, Q. Zhang, F. Liu, X. Wan, Y. Wang, W. Ni, G. Long, X. Yang, H. Feng, Y. Zuo, M. Zhang, F. Huang, Y. Cao, T. P. Russell, and Y. Chen *J. Am. Chem. Soc.* 2015, **137**, 3886–3893.
- (11) A. R. B. M. Yusoff, D. Kim, H. P. Kim, F. K. Shneider, W. J. da Silva, and J. Jang *Energy Environ. Sci.* 2015, **8**, 303–316.
- (12) G. Yu, J. Gao, J. C. Hummelen, F. Wudl, and A. J. Heeger, *Science* 1995, **270**, 1789–1791.
- (13) N. S. Sariciftci, L. Smilowitz, A. J. Heeger, and F. Wudl, *Science* 1992, **258**, 1474–1476.
- (14) L. Dou, J. You, J. Yang, C. -C. Chen, Y. He, S. Murase, T. Moriarty, K. Emery, G. Li, and Y. Yang, *Nat. Photonics* 2012, **6**, 180–185.
- (15) H. -Y. Chen, J. Hou, S. Zhang, Y. Liang, G. Yang, Y. Yang, L. Yu, Y. Wu, and G. Li, *Nat. Photonics* 2009, **3**, 649–653.
- (16) Y. Sun, G. C. Welch, W. L. Leong, C. J. Takacs, G. C. Bazan, and A. J. Heeger, *Nat. Mater.* 2012, **11**, 44–48.
- (17) J. Roncali, P. Leriche, and P. Blanchard, *Adv. Mater.* 2014, **26**, 3821–3838.
- (18) Y. Liu, C. -C. Chen, Z. Hong, J. Gao, Y. Yang, H. Zhou, L. Dou, G. Li, and Y. Yang, *Sci. Rep.* 2013, **3**, 3356/1–3356/8.

- (19) B. Kan, Q. Zhang, M. Li, X. Wan, W. Ni, G. Long, Y. Wang, X. Yang, H. Feng, and Y. Chen, *J. Am. Chem. Soc.* 2014, **136**, 15529-15532.
- (20) Q. Zhang, B. Kan, F. Liu, G. Long, X. Wan, X. Chen, Y. Zuo, W. Ni, H. Zhang, M. Li, Z. Hu, F. Huang, Y. Cao, Z. Liang, M. Zhang, T. P. Russell, and Y. Chen, *Nature photonics* 2015, **9**, 35-38.
- (21) Heliatek Consolidates its Technology Leadership by Establishing a New World Record for Organic Solar Technology with a Cell efficiency of 12%. "Heliatek GmbH, press release, 16th January, 2013, http://www.heliatek.com/newscenter/latest_news/neuer-weltrekord-fur-organische-solarzellen-heliatek-behauptet-sich-mit-12-zelleffizienz-als-technologiefuhrer/?lang=en (accessed July 22,2014).
- (22) Y. Lin, Y. Li, and X. Zhan, *Chem. Soc. Rev.* 2012, **41**, 4245-4272.
- (23) R. Fitzner, E. Mena-Osteritz, A. Mishra, G. Schulz, E. Reinold, M. Weil, C. Körner, H. Ziehlke, C. Elschner, K. Leo, M. Riede, M. Pfeiffer, C. Urich, and P. Bäuerle, *J. Am. Chem. Soc.* 2012, **134**, 11064-11067.
- (24) Z. Li, G. He, X. Wan, Y. Liu, J. Zhou, G. Long, Y. Zuo, M. Zhang, and Y. Chen, *Adv. Energy Mater.* 2012, **2**, 74-77.
- (25) J. Zhou, X. Wan, Y. Liu, Y. Zuo, Z. Li, G. He, G. Long, W. Ni, C. Li, X. Su, and Y. Chen, *J. Am. Chem. Soc.* 2012, **134**, 16345-16351.
- (26) M. Velusamy, J. -H. Huang, Y. -C. Hsu, H. -H. Chou, K. -C. Ho, P. -L. Wu, W. -H. Chang, J. T. Lin, and C. -W. Chu, *Org. Lett.* 2009, **11**, 4898-4901.
- (27) A. Leliège, P. Blanchard, T. Rousseau, and J. Roncali, *Org. Lett.* 2011, **13**, 3098-3101.
- (28) G. D. Sharma, M. Anil Reddy, K. Ganesh, S. P. Singh, and M. Chandrasekharam, *RSC Adv.* 2014, **4**, 732-742.
- (29) M. Chandrasekharam, M. Anil Reddy, K. Ganesh, G. D. Sharma, S. P. Singh, and J. Laxmikanth Rao, *Organic Electronics* 2014, **15**, 2116-2125.
- (30) B. Walker, A. B. Tamayo, X. -D. Dang, P. Zalar, J. H. Seo, A. Garcia, M. Tantiwivat and T. -Q. Nguyen. *Adv. Funct. Mater* 2009, **19**, 3063-3069
- (31) V. S. Gevaerts, E. M. Herzig, M. Kirkus, K. H. Hendriks, M. M. Wienk, J. Perlich, P. Müller-Buschbaum and R. A. J. Janssen. *Chem. Mater.* 2014, **26**, 916-926.
- (32) T. -Y. Chu, J. Lu, S. Beaupré, Y. Zhang, J. -R. Pouliot, J. Zhou, A. Najari, M. Leclerc, and Y. Tao, *Adv. Funct. Mater.* 2012, **22**, 2345-2351.
- (33) I. Osaka, T. Kakara, N. Takemura, T. Koganezawa, and K. Takimiya, *J. Am. Chem. Soc.* 2013, **135**, 8834-8837.

- (34) B. Wang, J. Zhang, H. L. Tam, B. Wu, W. Zhang, M. S. Chan, F. Pan, G. Yu, F. Zhu, and M. S. Wong, *Polym. Chem.* 2014, **5**, 836-843.
- (35) L. Dou, J. You, Z. Hong, Z. Xu, G. Li, R. A. Street, and Y. Yang, *Adv. Mater.* 2013, **25**, 6642-6671.
- (36) Y. Li, *Acc. Chem. Res.* 2012, **45**, 723-733.
- (37) S. D. Dimitrov, and J. R. Durrant, *Chem. Mater.* 2014, **26**, 616-630.
- (38) R. B. Zerdan, N. T. Shewmon, Y. Zhu, J. P. Mudrick, K. J. Chesney, J. Xue, and R. K. Castellano, *Adv. Funct. Mater.* 2014, **24**, 5993-6004
- (39) I. Meager, R. S. Ashraf, S. Mollinger, B. C. Schroeder, H. Bronstein, D. Beatrup, M. S. Vezie, T. Kirchartz, A. Salleo, J. Nelson, and I. McCulloch, *J. Am. Chem. Soc.* 2013, **135**, 11537-11540.
- (40) T. Lei, J. H. Dou, and J. Pei, *Adv. Mater.* 2012, **24**, 6457-6461.
- (41) X. L. Hu, L. J. Zuo, W. F. Fu, T. T. Larsen-Olsen, M. Helgesen, E. Bundgaard, E. Hagemann, M. M. Shi, F. C. Krebs, and H. Z. J. Chen, *Mater. Chem.* 2012, **22**, 15710-15716.
- (42) G. D. Sharma, J. A. Mikroyannidis, S. S. Sharma, M. S. Roy, and K. R. J. Thomas, *Org. Electron.* 2012, **13**, 652-666.
- (43) H. Chen, Y. Guo, G. Yu, Y. Zhao, J. Zhang, D. Gao, H. Liu, and Y. Liu, *Adv. Mater.* 2012, **24**, 4618-4622.
- (44) H. Bronstein, Z. Chen, R. S. Ashraf, W. Zhang, J. Du, J. R. Durrant, P. S. Tuladhar, K. Song, S. E. Watkins, Y. Geerts, M. M. Wienk, R. A. J. Janssen, T. Anthopoulos, H. Sirringhaus, M. Heaney, and I. McCulloch, *J. Am. Chem. Soc.* 2011, **133**, 3272-3275.
- (45) J. H. Dou, Y. Q. Zheng, T. Lei, S. D. Zhnag, Z. Wang, W. B. Zhang, J. Y. Wang, and J. Pei, *Adv. Funct. Mater.* 2014, **24**, 6270-6278.
- (46) Y. Lin, P. Cheng, Y. Li, and X. Zhan, *Chem. Commun.* 2012, **48**, 4773-4775.
- (47) D. Fernández, A. Viterisi, J. W. Ryan, F. G. Guirado, S. Vidal, S. Filippone, N. Martín, and E. Palomares, *Nanoscale* 2014, **6**, 5871-5878.
- (48) L. Dou, J. Gao, E. Richard, J. You, C. -C. Chen, K. C. Cha, Y. He, G. Li, and Y. Yang, *J. Am. Chem. Soc.* 2012, **134**, 10071-10079.
- (49) A. T. Yiu, P. M. Beaujuge, O. P. Lee, C. H. Woo, M. F. Toney, and J. M. J. Frechet, *J. Am. Chem. Soc.* 2012, **134**, 2180-2185.
- (50) R. S. Ashraf, I. Meager, M. Nikolka, M. Kirkus, M. Planelles, B. C. Schroeder, S. Holliday, M. Hurhangee, C. B. Nielsen, H. Sirringhaus, and I. McCulloch, *J. Am. Chem. Soc.* 2015, **137**, 1314-1321

- (51) Y. Lin, L. Ma, Y. Li, Y. Liu, D. Zhu, and X. Zhan, *Adv. Energy Mater.* 2013, **3**, 1166–1170.
- (52) J. Liu, Y. Sun, P. Moonsin, M. Kuik, C. M. Proctor, J. Lin, B. B. Hsu, V. Promarak, A. J. Heeger, and T. -Q. Nguyen, *Adv. Mater.* 2013, **25**, 5898-5903.
- (53) A. C. Rochat, L. Cassar, and A. Iqbal, *European Patent*, 0094911, 1983.
- (54) A. Tamayo, T. Kent, M. Tantitawat, M. A. Dante, J. Rogers, and T. -Q. Nguyen, *Energy Environ. Sci.* 2009, **2**, 1180-1186.
- (55) R. B. Zerdan, N. T. Shewmon, Y. Zhu, J. P. Mudrick, K. J. Chesney, J. Xue, and R. K. Castellano, *Adv. Funct. Mater.* 2014, **24**, 5993-6004.
- (56) J. L. Bredas, J. E. Norton, J. Cornil, and V. Coropceanu, *Acc. Chem. Res.* 2009, **42**, 1691–1699.
- (57) J. M. Halls, J. Cornill, D. A. dos Santos, R. Silbey, D. -H. Hwang, A. B. Holmes, J. L. Bredas, and R. H. Friend, *Phys. Rev. B* 1999, **60**, 5721–5727.
- (58) C. J. Brabec, C. Winder, N. S. Sariciftci, J. C. Humme-len, A. Dhanabalan, P. A. Van Hal, and R. A. J. Janssen, *Adv. Funct. Mater.* 2002, **12**, 709–712.
- (59) J. H. Hou, H. Y. Chen, S. Zhang, G. Li, and Y. Yang, *J. Am. Chem. Soc.* 2008, **130**, 16144–16145.
- (60) W. Ni, M. Li, X. Wan, H. Feng, B. Kan, Y. Zuo, and Y. Chen, *RSC Adv.* 2014, **4**, 31977-31980.
- (61) C. D. Wessendorf, G. L. Schulz, A. Mishra, P. Kar, I. Ata, M. Weidelener, M. Urdanpilleta, J. Hanisch, E. M. Osteritz, M. Lindén, E. Ashlswede, and P. Bäuerle, *Adv. Energy Mater.* 2014, **4**, 1400266/1-1400266/10.
- (62) Y. Matsuo, Y. Sato, T. Niinomi, I. Soga, H. Tanaka, and E. Nakamura, *J. Am. Chem. Soc.* 2009, **131**, 16048–16050.
- (63) M. -C. Yuan, M. -Y. Chiu, S. -P. Liu, C. -M. Chen, and K. -H. Wei, *Macromolecules* 2010, **43**, 6936–6938.
- (64) K. Vandewal, K. Tvingstedt, A. Gadisa, O. Inganas, and J. V. Manca, *Nat. Mater.* 2009, **8**, 904–909.
- (65) G. Long, X. Wan, B. Kan, Y. Liu, G. He, Z. Li, Y. Zhang, Y. Zhang, Q. Zhang, M. Zhang, and Y. Chen, *Adv. Energy Mater.* 2013, **3**, 639–646.
- (66) M. He, W. Han, J. Ge, W. Yu, Y. Yang, F. Qiu, and Z. Lin, *Nanoscale* 2011, **3**, 3159-3163.
- (67) U. Zhokhavets, T. Erb, G. Gobsch, M. Al-Ibrahim, and O. Ambacher, *Chem. Phys. Lett.* 2006, **418**, 347-350.

- (68) J. Liu, H. Choi, J. Y. Kim, C. Bailey, M. Durstock, and L. Dai, *Adv. Mater.* 2012, **24**, 538-542.
- (69) X. Yang, J. Loos, S. C. Veenstra, W. J. H. Verhees, M. M. Wienk, J. M. Kroon, M. A. J. Michels, and R. A. J. Janssen. *Nano Lett.* 2005, **5**, 579–583.
- (70) C. J. Brabec, N. S. Sariciftci, and J. C. Hummelen, *Adv. Funct. Mater.* 2001, **11**, 15–26.
- (71) B. Qi, and J. Wang, *Phys. Chem. Chem. Phys.* 2013, **15**, 8972–8982.
- (72) M. J. Frisch, G. W. Trucks, H. B. Schlegel, G. E. Scuseria, M. A. Robb, J. R. Cheeseman, G. Scalmani, V. Barone, B. Mennucci, and G. A. Petersson, Gaussian 09, Revision B.01, Gaussian, Inc., Wallingford, CT, 2010.
- (73) A. D. Becke, *J. Chem. Phys.*, 1993, **98**, 5648-5652.
- (74) A. D. Becke, *J. Chem. Phys.*, 1996, **104**, 1040.
- (75) G. A. Petersson, A. Bennett, T. G. Tensfeldt, M. A. Al-Laham, W. A. Shirley, and J. Mantzaris, *J. Chem. Phys.*, 1988, **89**, 2193-2198.
- (76) M. Cossi, V. Barone, R. Cammi, and J. Tomasi, *Chem. Phys. Lett.*, 1996, **255**, 327-335.
- (77) N. M. O'Boyle, A. L. Tenderholt, and K. M. Langner, *J. Comput. Chem.*, 2008, **29**, 839-845.

Table 1. Optical and electrochemical data of **CSDPP9-CSDPP12**

Dye	λ_{max}^a ($\epsilon \times 10^4$ $M^{-1}cm^{-1}$) (nm)	λ_{max} (nm) film	E_g^{opt} (eV) ^b	E_{ox} (V) ^c	E_{HOMO} (eV)	E_{0-0} (eV) ^d	E_{red} (V)	E_{LUMO} (eV) ^e
CSDPP9	561 (7.91)	588	1.88	0.92	-5.62	2.164	-1.246	-3.456
CSDPP10	579 (5.75)	614	1.82	0.81	-5.51	2.046	-1.241	-3.464
CSDPP11	609 (5.81)	632	1.74	0.70	-5.40	1.984	-1.282	-3.416
CSDPP12	597 (8.38)	624	1.78	0.84	-5.54	2.016	-1.172	-3.524

^aAbsorption spectra were recorded in DCM solutions at 298K.

^boptical bandgap estimated from the onset absorption edge of absorption spectra in thin film.

^cThe oxidation potentials (E_{ox} vs Ag/AgCl) of these dyes are corresponding to the HOMO levels.

^d E_{0-0} , was derived from the intersection of the absorption and emission spectra.

^e $E_{LUMO} = E_{HOMO} + E_{0-0}$.

Table 2. Calculated properties of the **CSDPP9-CSDPP12** using B3LYP/6-311G(d,p). Specifically HOMO and LUMO energies (eV), HOMO–LUMO gap (eV), HLG, with corresponding oscillator strengths, f , the wavelengths of the first excitation and excitations with the largest oscillator strengths and the dipole moment (D), μ .

CSDPPs	λ_{\max}^a (nm)	λ_{\max} (nm)	HOMO	LUMO	HLG	f	μ (D)
CSDPP9	561	534	-5.32	-2.77	2.55	0.76	0.36
CSDPP10	579	577	-5.17	-2.78	2.39	1.07	2.26
CSDPP11	609	598	-5.17	-2.79	2.32	1.16	3.27
CSDPP12	597	585	-5.21	-2.85	2.36	1.06	0.20

^a absorption values obtained from experimental data.

Table 3. Photovoltaic performances based on **CSDPP9-CSDPP12** small molecules blended with PC₇₁BM, weight ratio was 1:1 and processed from DCM solvent.

DPP	J_{sc} (mA/cm ²)	V_{oc} (V)	FF	PCE (%)	μ (cm ² /Vs)	R_s (Ω cm ²)	R_{sh} (Ω cm ²)
CSDPP9:PC₇₁BM	7.38	1.02	0.38	2.86	2.34x10 ⁻⁶	68	568
CSDPP10:PC₇₁BM	7.68	0.94	0.40	2.89	2.56x10 ⁻⁶	65	588
CSDPP11:PC₇₁BM	9.18	0.88	0.44	3.55	6.78x10 ⁻⁶	43	469
CSDPP12:PC₇₁BM	8.12	0.94	0.40	3.05	4.67x10 ⁻⁶	48	418

Table 4. Photovoltaic performances based on **CSDPP11:PC₇₁BM** and **CSDPP12:PC₇₁BM** active layer with different treatments

Active layer	J_{sc} (mA/cm ²)	V_{oc} (V)	FF	PCE (%)	μ (cm ² /Vs)	R_s (Ω cm ²)	R_{sh} (Ω cm ²)
CSDPP11:PC₇₁BM^a	9.98	0.86	0.54	4.63	3.58 x10 ⁻⁵	26	590
CSDPP12:PC₇₁BM^a	8.88	0.90	0.52	4.15	1.03 x10 ⁻⁵	32	582
CSDPP11: PC₇₁BM^b	10.86	0.84	0.60	5.47	8.89 x10 ⁻⁵	16	678
CSDPP12: PC₇₁BM^b	9.92	0.88	0.56	4.88	6.46x10 ⁻⁵	22	665

^aTA

^bSATA

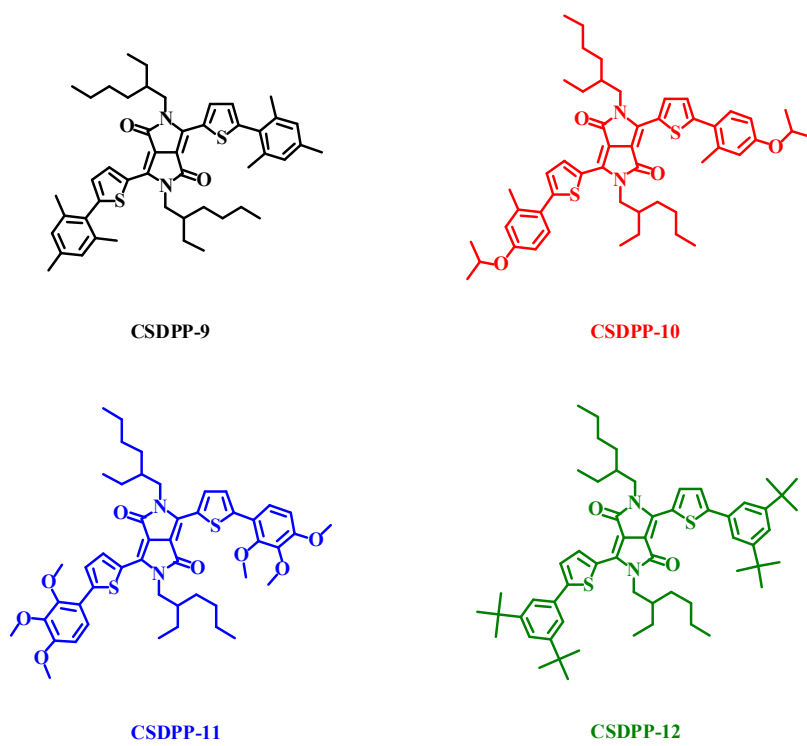


Figure 1. Structures of CSDPP9-CSDPP12

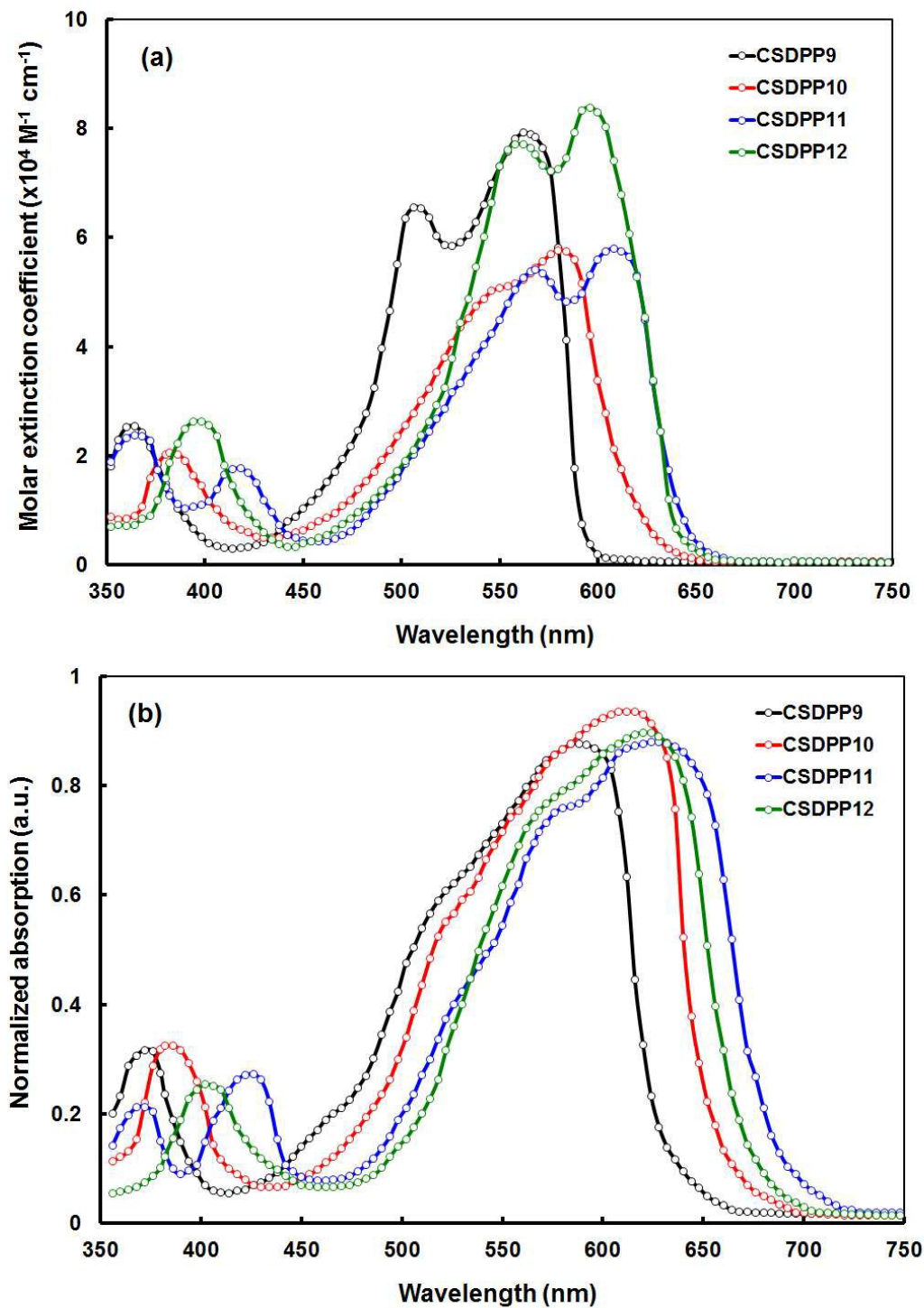


Figure 2. (a) UV/Vis absorption spectrum of the CSDPP9, CSDPP10, CSDPP11 and CSDPP12 small molecules in DCM and (b) in thin film.

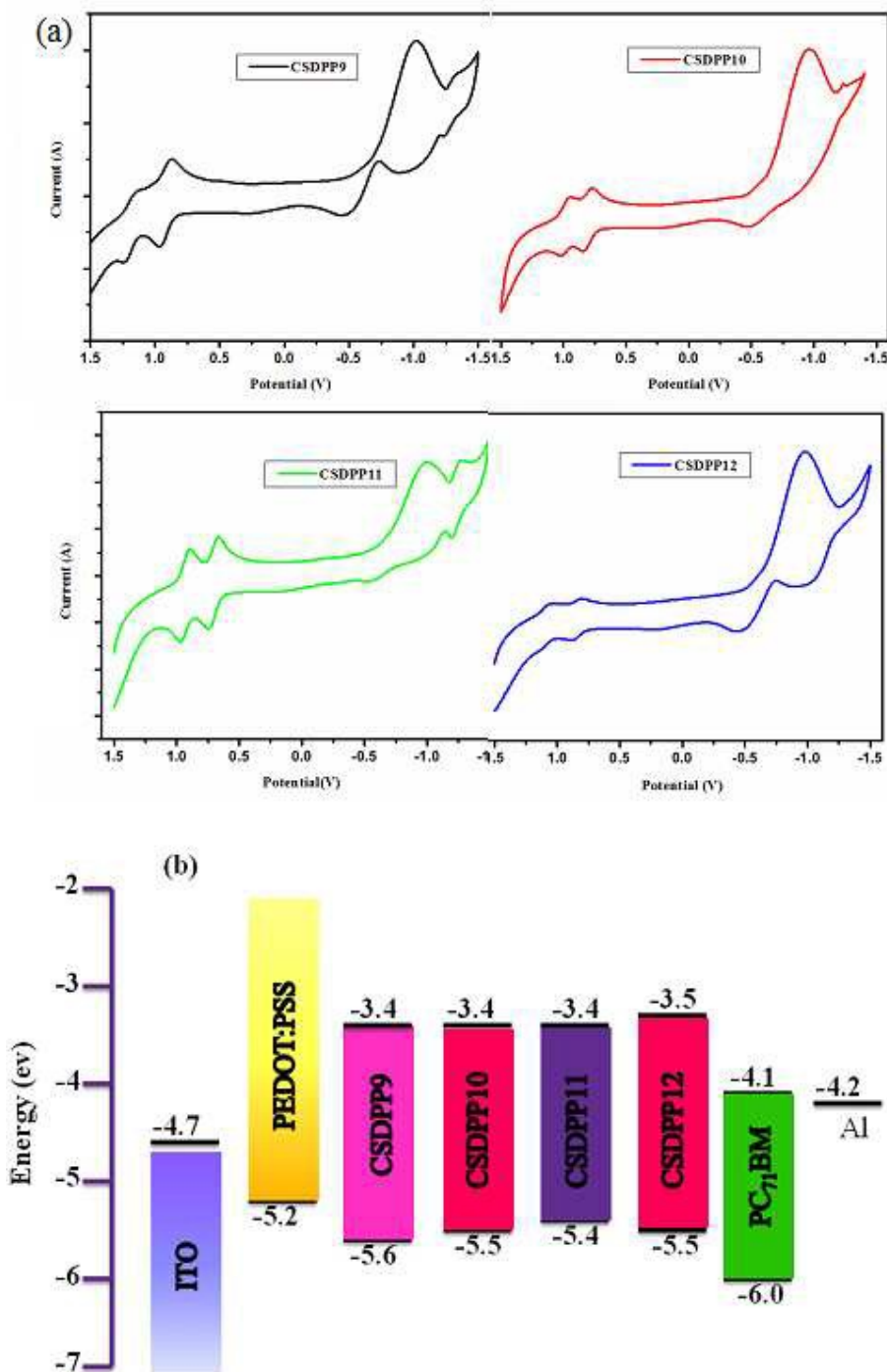


Figure 3. (a) Cyclic voltammograms of CSDPP9, CSDPP10, CSDPP11 and CSDPP12 in DCM; scan rate 100 mV s^{-1} ; supporting electrolyte: tetrabutylammonium hexafluorophosphate (NBu_4PF_6). (b) Energy levels of different components in a photovoltaic device.

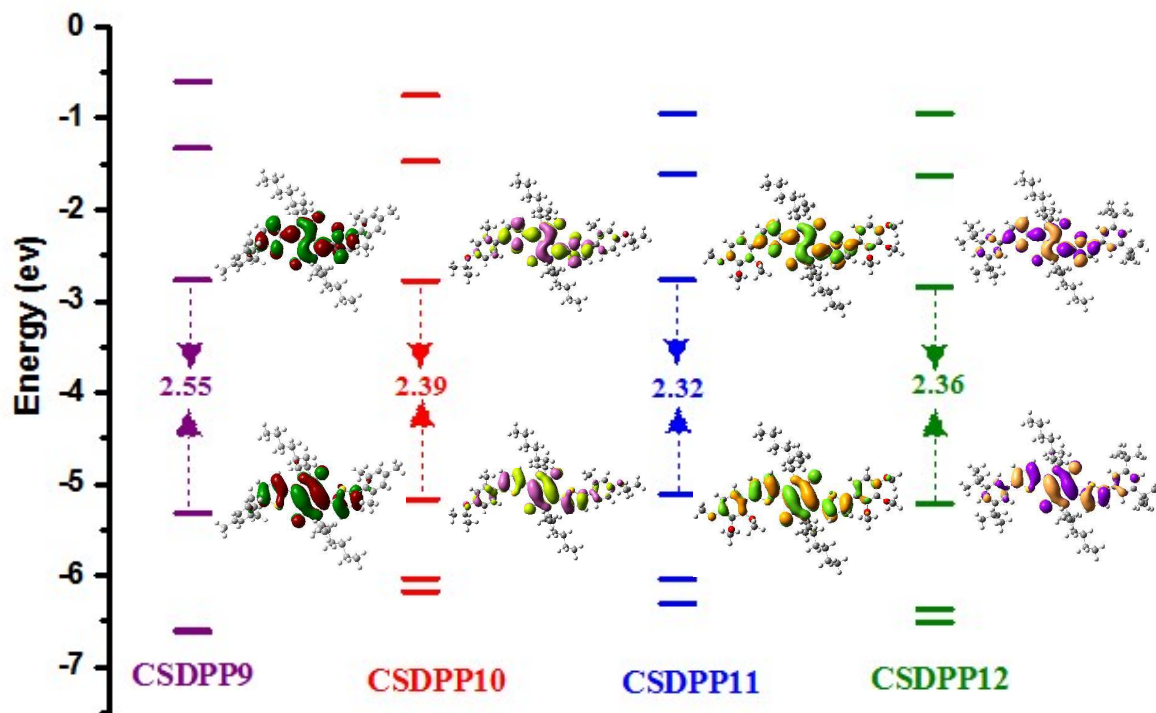


Figure 4. Calculated HOMO–LUMO gaps at B3LYP/6-311G(d, p) level of theory and respective HOMO and LUMO orbital pictures at B3LYP/6-311G(d, p)level of **CSDPPs** in DCM solvent.

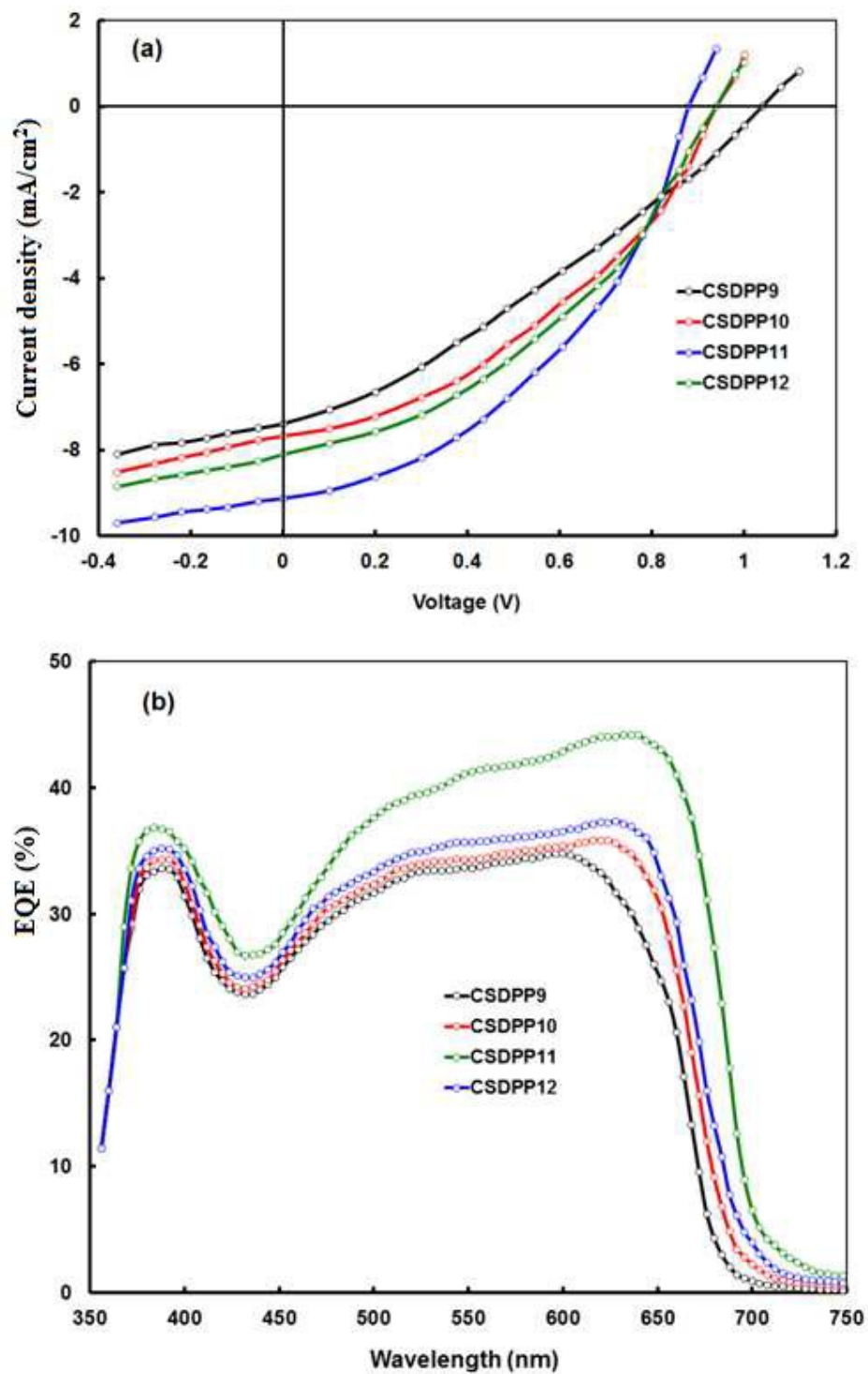


Figure 5. (a) Current density–voltage characteristics (under AM 1.5G, 100 mW/cm² illumination) and (b) EQE spectra of CSDPP9, CSDPP10, CSDPP11 and CSDPP12.

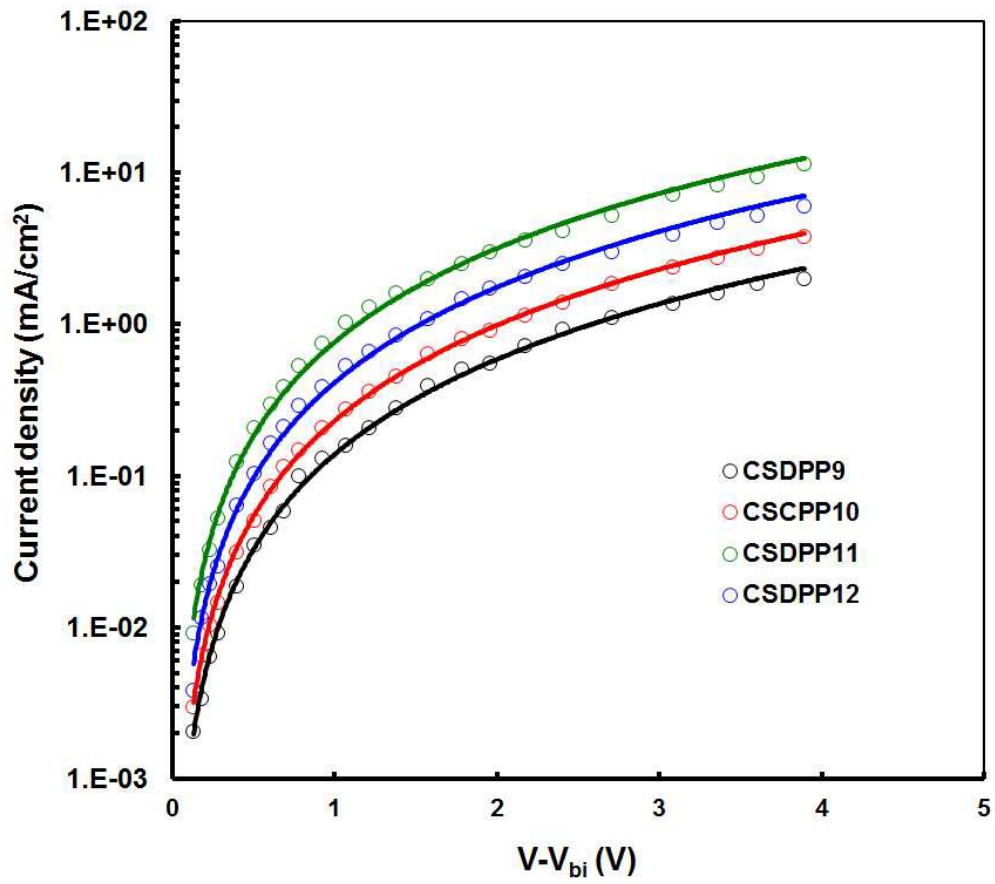


Figure 6. J-V characteristics of hole only devices for different **DPPs** blended with PC₇₁BM.

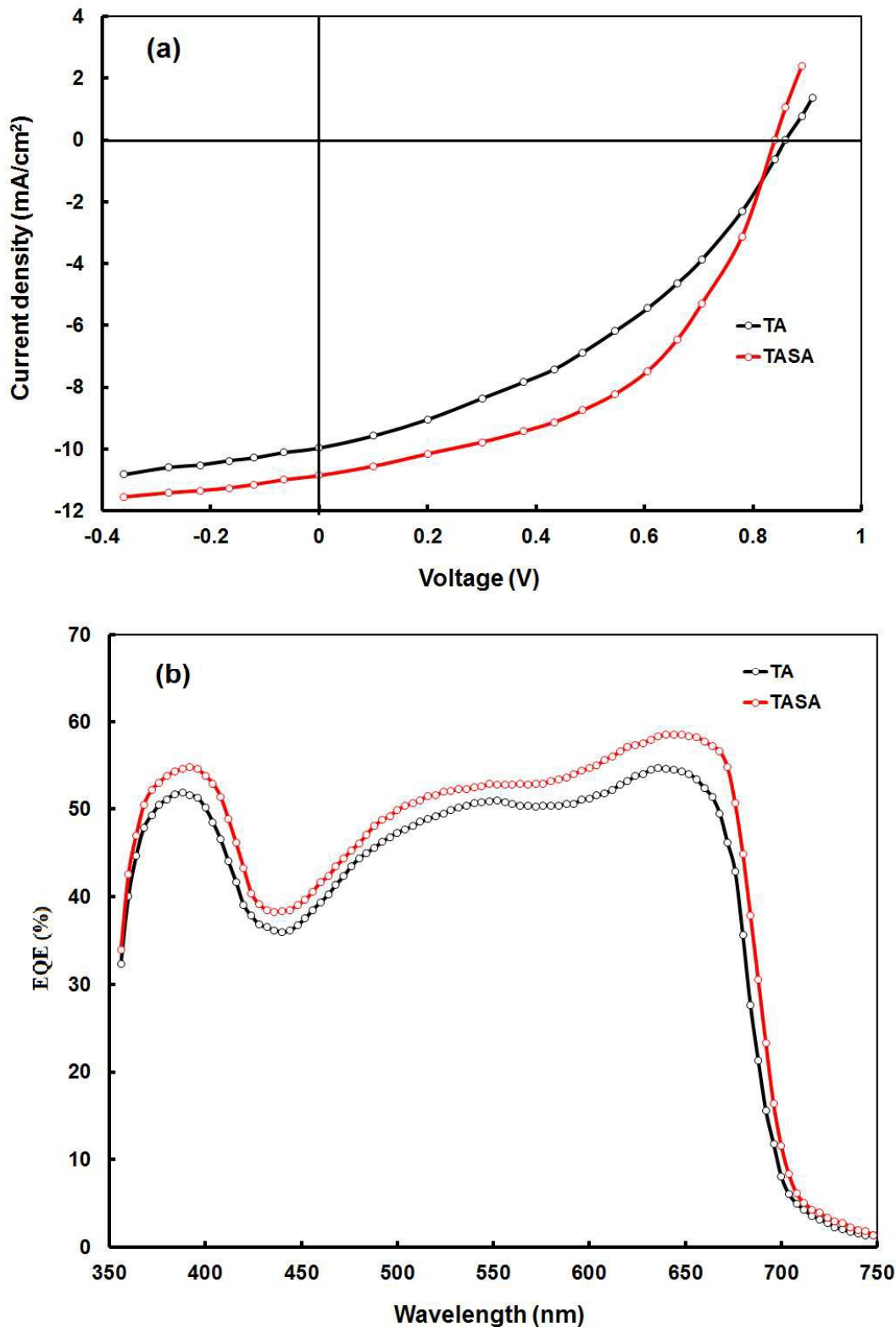


Figure 7. Current density–voltage characteristics (under AM 1.5G, 100 mW/cm² illumination) (a) J-V spectra of OSC devices based on CSDPP11:PC₇₁BM with TA and SATA treatments and (b) EQE spectra of OSC devices based on CSDPP11:PC₇₁BM with TA and SATA treatments

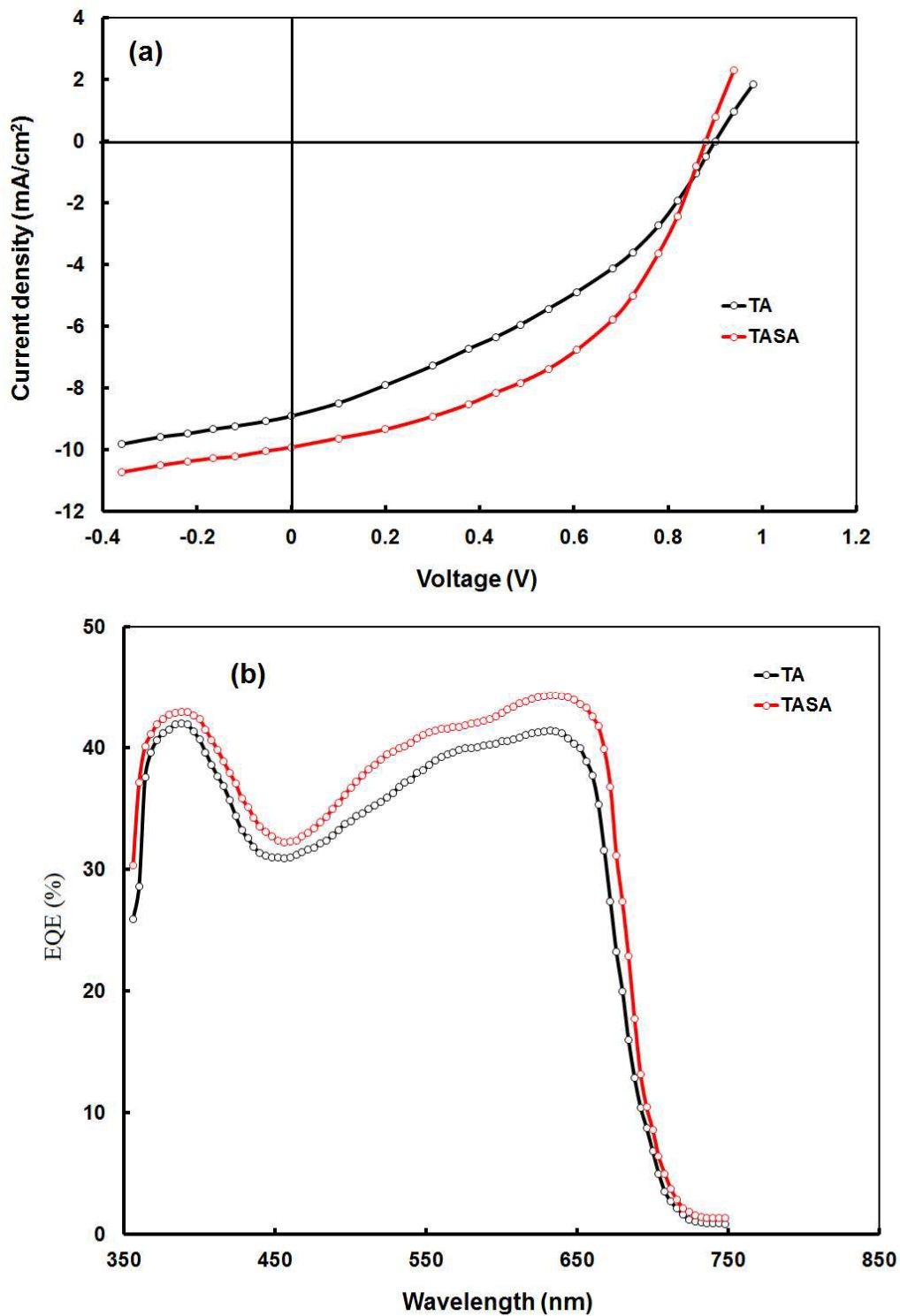


Figure 8. Current density–voltage characteristics (under AM 1.5G, 100 mW/cm² illumination) (a) J-V spectra of OSC devices based on CSDPP12:PC₇₁BM with TA and SATA treatments and (b) EQE spectra of OSC devices based on CSDPP12:PC₇₁BM with TA and SATA treatments

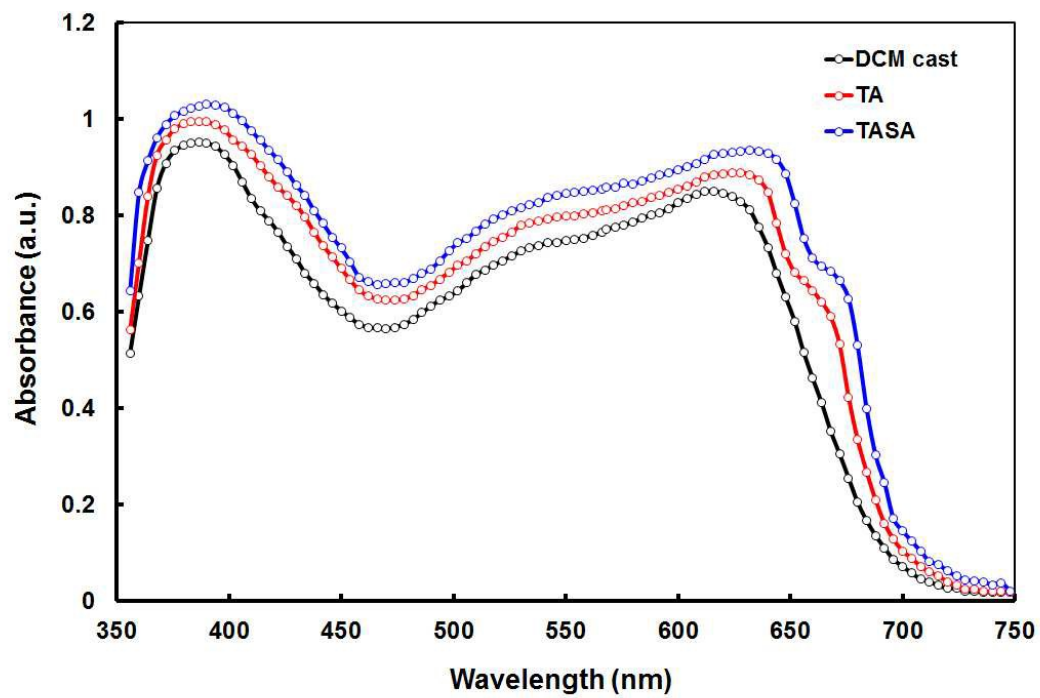


Figure 9. Absorption of CSDPP11:PC71BM as cast, TA and SATA treatments

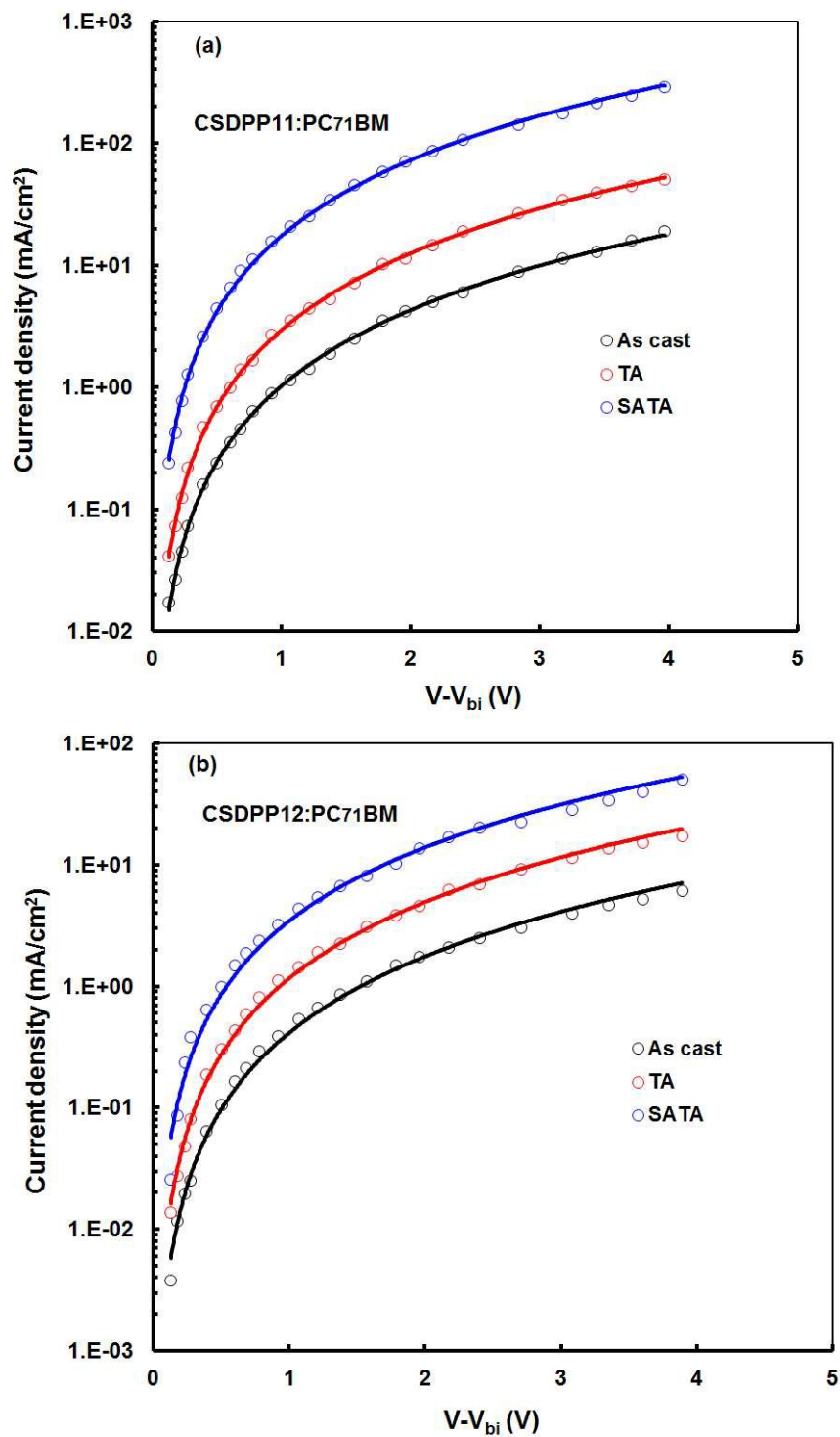


Figure 10. J-V characteristics of hole only devices for (a) CSDPP11:PC₇₁BM and (b) CSDPP12:PC₇₁BM active layer (as cast, TA and SATA treatments).

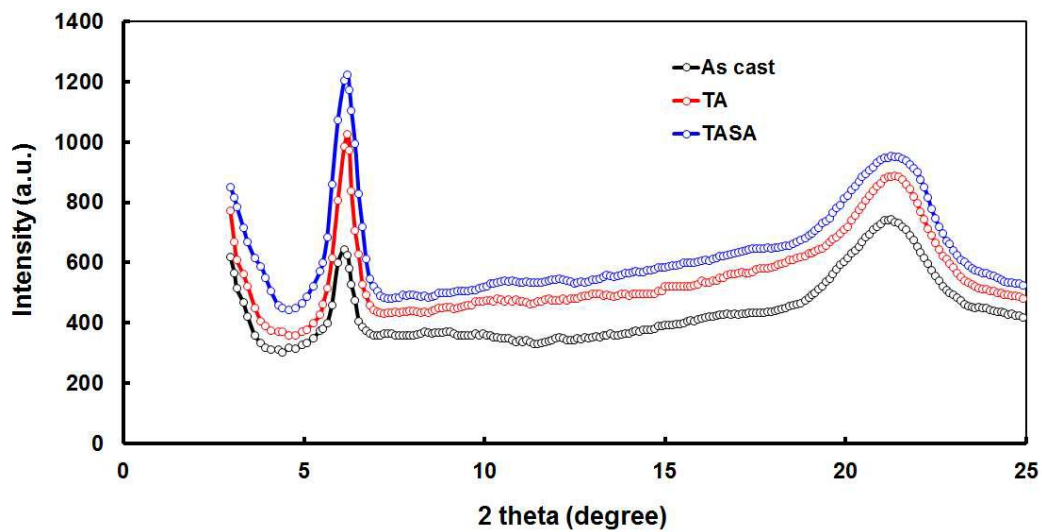


Figure 11. XRD patterns of CSDPP11:PC₇₁BM blend films spin-coated from DCM onto glass substrate with different post treatment.

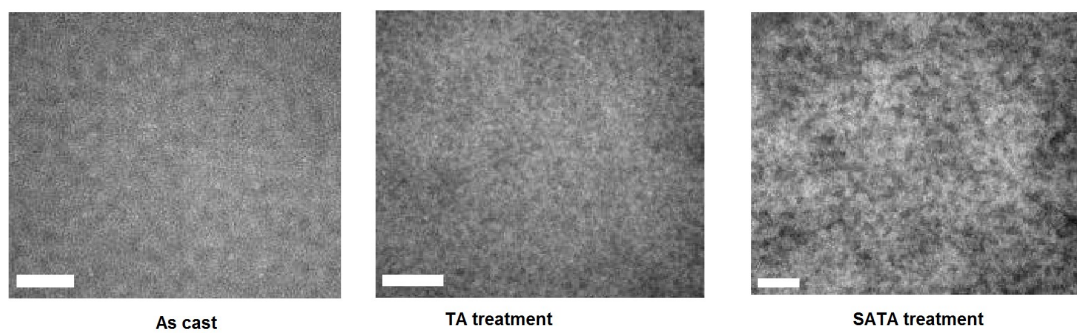


Figure 12. TEM images of CSDPP11:PC₇₁BM blend films, i.e. as cast, TA treatment and SATA treatment

TOC

